Cancer Research

Antitumor Activity of Metal-Chelating Compound Dp44mT Is Mediated by Formation of a Redox-Active Copper Complex That Accumulates in Lysosomes

David B. Lovejoy[1], Patric J. Jansson[1], Ulf T. Brunk[1,2], Jacky Wong[1], Prem Ponka[3], and Des R. Richardson[1]

Abstract

The metal-chelating compound Dp44mT is a di-2-pyridylketone thiosemicarbazone (DpT) which displays potent and selective antitumor activity. This compound is receiving translational attention, but its mechanism is poorly understood. Here, we report that Dp44mT targets lysosome integrity through copper binding. Studies using the lysosomotropic fluorochrome acridine orange established that the copper–Dp44mT complex (Cu[Dp44mT]) disrupted lysosomes. This targeting was confirmed with pepstatin A–BODIPY FL, which showed redistribution of cathepsin D to the cytosol with ensuing cleavage of the proapoptotic BH3 protein Bid. Redox activity of Cu[Dp44mT] caused cellular depletion of glutathione, and lysosomal damage was prevented by cotreatment with the glutathione precursor *N*-acetylcysteine. Copper binding was essential for the potent antitumor activity of Dp44mT, as coincubation with nontoxic copper chelators markedly attenuated its cytotoxicity. Taken together, our studies show how the lysosomal apoptotic pathway can be selectively activated in cancer cells by sequestration of redox-active copper. Our findings define a novel generalized strategy to selectively target lysosome function for chemotherapeutic intervention against cancer. *Cancer Res; 71(17); 5871–80. ©2011 AACR.*

Introduction

Neoplastic cells have high requirements for iron (Fe) due to their generally higher rates of proliferation than normal cells (1). In fact, neoplastic cells express enhanced transferrin receptor 1 (TfR1) levels relative to their normal counterparts (2) and take up Fe from transferrin (Tf) at a rapid rate (3), making them selectively sensitive to Fe chelation. Cancer cells also take up more copper (Cu) than their normal counterparts, as this metal is essential for angiogenesis and metastasis (4).

Considering the crucial roles of these metals, development of novel Fe and Cu chelators has become a promising anticancer strategy (1, 5). Indeed, the chelator, Triapine (3-aminopyridine-2-carboxaldehyde thiosemicarbazone; Fig. 1), which inhibits tumor growth, has entered clinical trials (1). However, the di-2-pyridylketone thiosemicarbazone (DpT) chelators possess far greater antitumor activity and selectivity than Triapine (6, 7).

Authors' Affiliations: [1]Department of Pathology, University of Sydney, Sydney, New South Wales, Australia; [2]Department of Pharmacology, Linköping University, Linköping, Sweden; and [3]Lady Davis Institute, Montreal, Quebec, Canada

Note: Supplementary data for this article are available at Cancer Research Online (http://cancerres.aacrjournals.org/).

D.B. Lovejoy and P.J. Jansson contributed equally to the study.

Corresponding Author: Des R. Richardson, The University of Sydney, Blackburn Building D06, Sydney, New South Wales 2006, Australia. Phone: 61-2-9036-6548; Fax: 61-2-9036-6549; E-mail: d.richardson@sydney.edu.au

doi: 10.1158/0008-5472.CAN-11-1218

One of the most effective DpT chelators is di-2-pyridylketone-4,4,-dimethyl-3-thiosemicarbazone (Dp44mT; Fig. 1; ref. 6). Dp44mT shows marked and selective activity against tumor xenografts in mice (6, 7). The proposed mechanism of action of Dp44mT involves Fe chelation and redox cycling of its Fe complex to generate reactive oxygen species (ROS; refs. 6, 8, 9). The potent and antitumor activity of Dp44mT has been verified by others (10–12). In particular, Rao and colleagues reported topoisomerase IIα inhibition (10) and broad and specific antitumor activity (12). Additional modes of anticancer activity reported for Dp44mT include inhibition of the metastasis suppressor protein, Ndrg-1 (1), and modulation of the cell-cycle control proteins of the cyclin family (A, B, D1, D2, and D3) as well as cyclin-dependent kinase 2 (1, 5).

Dp44mT not only binds Fe, but also Cu, and both complexes are redox active, contributing to their marked cytotoxicity (13). Considering: (i) the potential of lysosomes as a therapeutic target; (ii) their key role in metal metabolism (14, 15); and (iii) their pronounced susceptibility to ROS (15, 16), our goals were to examine the effects of the DpT compounds on Cu and Fe and their interaction with lysosomes. Our work has elucidated a novel strategy for the design of new therapeutics that activate the lysosomal apoptotic pathway by binding redox-active Cu.

Materials and Methods

Chemicals

2-Hydroxy-1-naphthaldehyde isonicotinoyl hydrazone (311), di-2-pyridylketone-2-methyl-3-thiosemicarbazone (Dp2mT), di-

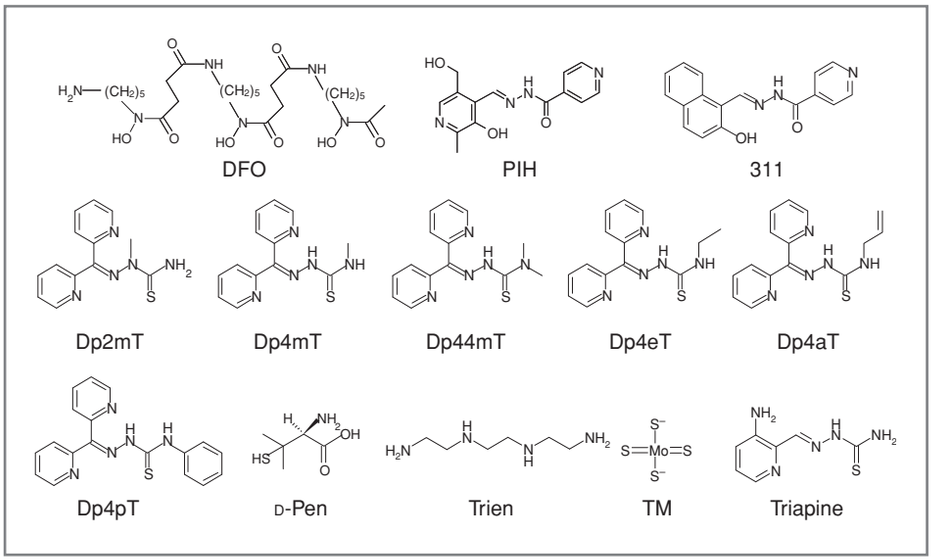

Figure 1. Chelator structures.

2-pyridylketone-4-ethyl-3-thiosemicarbazone (Dp4eT), di-2-pyridylketone-4-allyl-3-thiosemicarbazone (Dp4aT), di-2-pyridylketone-4-methyl-3-thiosemicarbazone (Dp4mT), Dp44mT, di-2-pyridylketone-4-phenyl-3-thiosemicarbazone (Dp4pT), and pyridoxal isonicotinoyl hydrazone (PIH) were synthesized as described (6, 8). Desferrioxamine (DFO) was from Novartis. Buthionine sulfoximine (BSO), D-penicillamine (D-pen), tetrathiomolybdate (TM), and Trientine (Trien) were purchased from Sigma-Aldrich. Triapine was from Vion Pharmaceuticals.

Cell culture

Human SK-N-MC neuroepithelioma cells, MCF-7 breast cancer cells, DMS-53 lung carcinoma cells, and human umbilical vein endothelial cells (HUVEC) were obtained from the American Type Culture Collection and grown as described (17, 18). Cells were used within 2 months of purchase after resuscitation of frozen aliquots. Cell lines were authenticated on the basis of viability, recovery, growth, morphology, and also cytogenetic analysis, antigen expression, DNA profile, and isoenzymology by the provider.

Procedures involved in preparing ^{59}Fe-transferrin and conducting cytotoxicity assays have been described previously (17, 18).

^{64}Cu and ^{59}Fe efflux assays

Efflux studies examining the ability of chelators to mobilize ^{59}Fe or ^{64}Cu (10 μCi/mL; $^{64}CuCl_2$; ANSTO) from cells were done by standard methods (17). Briefly, cells were prelabeled for 3 hours at 37°C with ^{64}Cu (10 μCi) or ^{59}Fe-transferrin (^{59}Fe-Tf; 0.75 μmol/L), washed 4 times on ice and reincubated with medium (control) or medium and chelators (25 μmol/L) for up to 6 hours at 37°C and then harvested (17). Radioactivity was measured in the pellet and supernatant using a γ-scintillation counter (Wallac Wizard 3; Perkin Elmer).

Cellular retention of ^{64}Cu complexes

Complexes were prepared by adding equimolar ^{64}Cu and chelator. SK-N-MC cells were incubated with the complexes for 3 hours at 37°C, washed 4 times on ice, reincubated for 3 hours at 37°C in control media, and the percentage of ^{64}Cu remaining cell associated assessed (17).

Subcellular fractionation

SK-N-MC cells (3 × T175 flasks, 80% confluent) were prelabeled for 3 hours at 37°C with ^{64}Cu (10 μCi), washed and reincubated at 37°C with medium (control) or Dp44mT (5 μmol/L) for 3 hours at 37°C. Cells were added to extraction buffer (0.25 mol/L sucrose, 10 mmol/L Tris-HCl) and disrupted using a Dounce "B" homogenizer on ice. To prevent damage to the released lysosomes, disruption of cells was discontinued when approximately 50% of the intact cells were disrupted. The suspension was centrifuged 1,000 × *g* for 15 minutes at 4°C, the pellet discarded, and supernatant centrifuged at 16,000 × *g* for 15 minutes at 4°C to yield a crude lysosomal/mitochondrial fraction. As a further control, enzyme marker analysis for the lysosomal specific enzyme acid phosphatase (Sigma) showed that this fraction was enriched with lysosomes (as determined by spectrophotometric assessment at 405 nm).

Speciation studies

Potentiometric titrations were conducted as described (8).

Assessment of lysosomal membrane permeability

Distribution of acridine orange (Sigma) was used to determine lysosomal membrane permeability (LMP) as previously reported (18) and was quantified by flow cytometry (19). Briefly, cells were incubated for 15 minutes at 37°C with acridine orange (20 μmol/L), washed 3 times with PBS, and then incubated for 30 minutes at 37°C with 25 μmol/L

chelator or reagent. Cathepsin D release was examined by fluorescence microscopy as previously reported (20) using a pepstatin A–BODIPY FL conjugate (Invitrogen) that selectively binds to cathepsin D. LysoTracker red (Invitrogen) was used to confirm colocalization of cathepsin D with lysosomes. For details, see Supplementary Methods.

Western blot analysis

Assessment of Bid cleavage was assessed by Western blotting by standard methods (6) using antibodies to Bid (Cell Signaling Technology) and β-actin (clone AC-1; Sigma).

Mitochondrial stability assay

Tetramethylrhodamine ethyl ester (TMRE; Invitrogen) partitions to the mitochondrial matrix (21). SK-N-MC cells were incubated with 20 nmol/L of TMRE for 0.25 hours at 37°C and then incubated with 5 μmol/L of Cu[Dp44mT] for 0.5 to 2 hours at 37°C. Mitochondrial damage was examined by flow cytometry (21).

GSH/GSSG assay

This assay was conducted using a kit (Calbiochem). SK-N-MC cells were treated at 25 μmol/L for up to 24 hours at 37°C with Cu(II), Fe(III), Dp44mT, Cu[Dp44mT], or Fe[Dp44mT]$_2$. As a control, BSO (100 μmol/L) was added as a glutathione synthesis inhibitor (22).

Redox studies: oxidation of H_2DCF

Studies without cells were conducted as described with H_2DCF (5 μmol/L; ref. 23). As a positive control, Fe(III) at 5 μmol/L was reduced to Fe(II) using cysteine (100 μmol/L) in 150 mmol/L acetate buffer (pH = 5.0). Hydrogen peroxide (100 μmol/L) was then added to initiate hydroxyl radical generation. To confirm hydroxyl radical production, dimethyl sulfoxide (DMSO; 10% v/v) was used, as it has been reported to be an effective hydroxyl radical scavenger (24, 25). Cu[Dp44mT] and other reagents (at 5 μmol/L, except DMSO at 10% v/v) were added to examine hydroxyl radical production. Intracellular oxidation of H_2DCF studies were conducted as described in previous studies (6, 23).

Statistics

Data were compared using Student's *t* test. Results were expressed as mean ± SD (number of experiments) and considered to be statistically significant when $P < 0.05$.

Results

Active DpT chelators prevent ^{64}Cu mobilization but markedly induce ^{59}Fe efflux

To assess the antineoplastic mechanisms of the DpT analogues (Fig. 1), their ability to remove ^{64}Cu from prelabeled cells was compared with their interaction with ^{59}Fe. The activity of DpT chelators was compared with the Fe chelators, DFO, PIH, and 311 (17), and Cu chelators, D-pen, Trien, and TM (Fig. 1; ref. 1). The DpT chelators, Dp4mT, Dp44mT, Dp4eT, Dp4aT, and Dp4pT, were found to be ineffective at 25 μmol/L at inducing ^{64}Cu release from cells (leading to ^{64}Cu retention) relative to when cells were incubated with control medium (Fig. 2A). In these studies, SK-N-MC cells were used as their response to chelators is well characterized (6, 17).

The results above were in contrast to their ability to mobilize ^{59}Fe, where the DpT chelators significantly ($P < 0.001$) induced a more than 700% increase in ^{59}Fe release relative to control cells (Fig. 2B). Hence, there was a difference in the ability of DpT chelators to mobilize these metals. The only exception was the negative control, Dp2mT, which failed to induce significant ^{64}Cu or ^{59}Fe efflux (Fig. 2A and B). By design, Dp2mT cannot bind metals (6), showing the importance of metal binding for DpT chelator activity. The chelators DFO, PIH, and 311 were included as positive controls to increase ^{59}Fe efflux, and we also examined their effects on ^{64}Cu release. Only 311 showed a marked interaction with ^{64}Cu, significantly ($P < 0.001$) reducing its efflux to 43% ± 10% of the control (Fig. 2A). The Cu chelators, D-pen and Trien, were ineffective at inducing ^{64}Cu efflux at 25 μmol/L (Fig. 2A). However, the Cu chelator, TM, significantly ($P < 0.05$) reduced ^{64}Cu efflux to 76% ± 2% of the control. The low activity of the Cu chelators, D-pen, Trien, and TM, at mobilizing ^{64}Cu was unexpected on the basis of their *in vivo* efficacy (1). However, their mechanism of action in cell culture is unclear, and the efficacy *in vivo* could relate to extracellular rather than intracellular chelation (26). These efflux experiments were repeated using MCF-7 (Fig. 2C and D), and to provide a comparison with tumor cells, normal HUVECs were used (Fig. 2E and F). Generally, the active chelators accumulated ^{64}Cu similarly across the 3 cell types (Fig. 2A–F). In terms of the effect of Dp44mT on inhibiting ^{64}Cu release, its effect was greater in HUVECs and MCF-7 cells than SK-N-MC.

The kinetics of ^{64}Cu and ^{59}Fe release were assessed over a range of reincubation times (0.5–6 hours) using SK-N-MC cells and HUVECs that were prelabeled with ^{64}Cu or ^{59}Fe-Tf for 3 hours at 37°C (Supplementary Fig. S1A–D). These results showed that Dp44mT and 311 decreased ^{64}Cu release relative to the control while both ligands markedly increased ^{59}Fe efflux as a function of time. In addition, dose–response curves showed that 311 and Dp44mT decreased ^{64}Cu release compared with the control, leading to ^{64}Cu accumulation in cells (Supplementary Fig. S1E). With Dp44mT, this effect was reversible as its concentration increased to more than 5 μmol/L, and at these higher concentrations, cellular damage results in the release of the Cu–Dp44mT complex from the cells. In contrast, at lower concentrations, the cells are still intact preventing ^{64}Cu release. In terms of ^{59}Fe efflux, 311 and Dp44mT markedly increased cellular ^{59}Fe release as a function of concentration (Supplementary Fig. S1F). Collectively, the active DpT group of chelators markedly prevented ^{64}Cu efflux from all cell types, leading to ^{64}Cu accumulation.

Precomplexation of ^{64}Cu with 311 and the DpT ligands leads to intracellular accumulation of their ^{64}Cu complexes

The results indicating intracellular accumulation of DpT–^{64}Cu complexes were confirmed by studies where

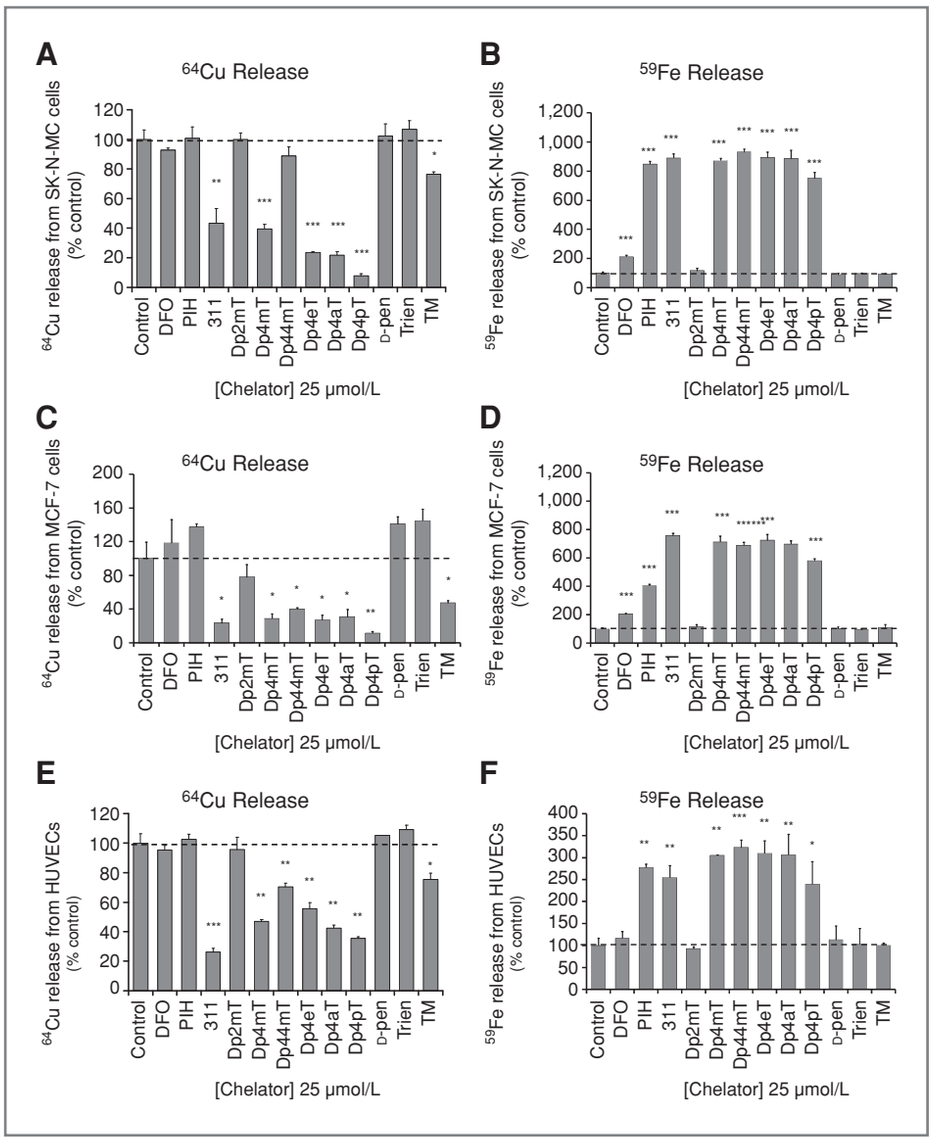

Figure 2. DpT chelators cause significant cellular accumulation of ^{64}Cu (A) but induce considerable ^{59}Fe release (B) from prelabeled SK-N-MC cells; (C and D) MCF-7 cells; and (E and F) HUVECs when incubated as described in Materials and Methods. Results are mean ± SD (3 experiments). *, versus control, $P < 0.05$; **, versus control, $P < 0.01$; ***, versus control, $P < 0.001$.

SK-N-MC cells were labeled for 3 hours at 37°C with preformed ^{64}Cu–chelator complexes. The cells were then washed and reincubated for 3 hours at 37°C in control media and the percentage of ^{64}Cu remaining cell associated then quantified. In control cells incubated with ^{64}Cu only, only 4% ± 1% of ^{64}Cu remained intracellular (Fig. 3A). Hence, most ^{64}Cu had been released during the reincubation. Cells labeled with the ^{64}Cu complexes of the active DpT analogues (Dp4mT, Dp44mT, Dp4eT, Dp4aT, and Dp4pT) and then reincubated with control medium, showed that 39% to 68% of ^{64}Cu remained cell associated (Fig. 3A). In contrast, ^{64}Cu complexes of Dp2mT, D-pen, and Trien were no more effective than the control at retaining intracellular ^{64}Cu (Fig. 3A). The ^{64}Cu–TM complex also led to intracellular ^{64}Cu accumulation relative to the control. These results explain the low efflux of ^{64}Cu observed with the active DpT analogues (Fig. 2A), as their ^{64}Cu complexes become "trapped" within cells.

Subcellular fractionation indicates ^{64}Cu[Dp44mT] accumulates within a crude lysosomal/mitochondrial fraction

To examine the subcellular localization of the accumulated ^{64}Cu, SK-N-MC cells were labeled for 3 hours at 37°C with ^{64}Cu, washed, and reincubated for 3 hours at 37°C with Dp44mT (5 μmol/L) or control media. The distribution of ^{64}Cu in the cytosol and crude lysosomal/mitochondrial fraction was examined by differential centrifugation. In cells reincubated with Dp44mT, a significantly ($P < 0.001$) greater proportion of ^{64}Cu accumulated in the lysosomal/mitochondrial fraction (Fig. 3B).

Considering this observation, we hypothesized that because of the polyprotic nature of Dp44mT (8), it was trapped in acidic lysosomes as it became positively charged. To assess this, speciation studies of the chelator as a function of pH were conducted. At a pH of 7.4, 100% of the ligand is in its neutral

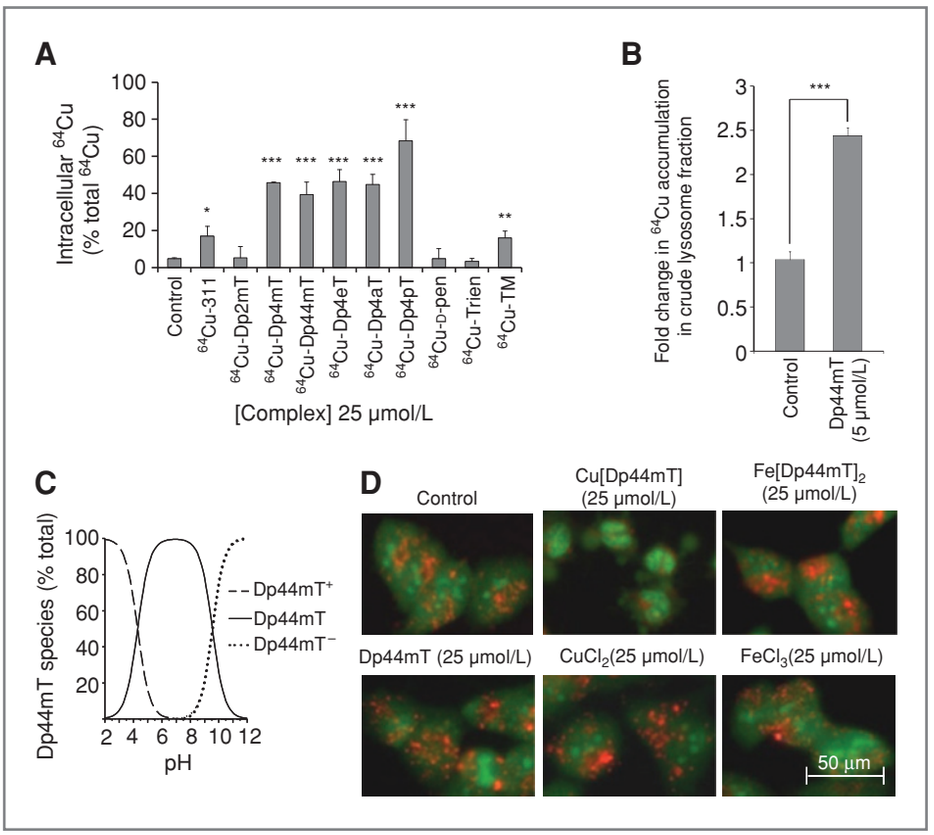

Figure 3. A, complexation of DpT chelators with ^{64}Cu leads to its cellular accumulation. Results represent intracellular ^{64}Cu (% total ^{64}Cu) expressed as mean ± SD (3 experiments). B, Dp44mT causes ^{64}Cu accumulation in a crude lysosome fraction. Results are mean ± SD (3 experiments). *, versus control, $P < 0.05$; **, versus control, $P < 0.01$; ***, versus control, $P < 0.001$. C, distribution of ionized species of Dp44mT as a function of pH. Results are typical of 3 experiments. D, a solution of 25 μmol/L of Cu[Dp44mT] disrupts lysosomal integrity after 0.5 hours at 37°C. Results are typical of 3 experiments. Scale bar, 50 μm.

state (Dp44mT), allowing facile transport through membranes, whereas at a lysosomal pH of 5, 16% is charged leading to lysosomal accumulation ($Dp44mT^+$; Fig. 3C). It should be noted that while 16% of the ligand is protonated at a pH of 5, this leads to accumulation of the ligand over time. This occurs due to the process of: (i) the neutral ligand entering the lysosome; (ii) the ligand becoming protonated and charged at lysosomal pH (pH = 5), preventing its passage out of the organelle; (iii) the charged ligand-binding copper in the lysosome; and (iv), as the so formed copper complex is probably positively charged, it also cannot escape the lysosome accounting for the ^{64}Cu accumulation in this compartment (see Fig. 3B).

Acridine orange indicates lysosomal permeabilization by Cu[Dp44mT]

To further explore the potential effect of Dp44mT and its Cu complex (Cu[Dp44mT]) on the lysosome, we implemented the lysosomotropic fluorophore, acridine orange (Fig. 3D) that accumulates within lysosomes (18). High lysosomal concentrations of acridine orange give a red fluorescence, whereas lower cytosolic and nuclear concentrations give a green fluorescence (18).

Examining control cells by fluorescence microscopy, a granular red fluorescence consistent with acridine orange concentration in lysosomes was found (Fig. 3D; ref. 18). However, incubation of cells with 25 μmol/L of Cu[Dp44mT] for 0.5 hours resulted in a marked loss of red fluorescence and the disappearance of red vesicles consistent with increased LMP, as well as the appearance of apoptotic bodies (Fig. 3D). In contrast, the $Fe[Dp44mT]_2$ complex, Dp44mT, $CuCl_2$, or $FeCl_3$ (at 25 μmol/L), had no significant effect relative to the control (Fig. 3D). The lack of activity of Dp44mT or $Fe[Dp44mT]_2$ is due to the short incubation period (0.5 hours) used, which was optimal for detecting the effect of Cu[Dp44mT]. Indeed, Dp44mT and $Fe[Dp44mT]_2$ only induce significant cytotoxicity after 24 hours (Fig. 6A). These data using fluorescence microscopy were confirmed upon quantification by flow cytometry, where only the Cu[Dp44mT] complex (25 μmol/L) significantly ($P < 0.001$) reduced red fluorescence (Supplementary Fig. S2).

To further examine the effect of Cu[Dp44mT] on the lysosome, we examined the intracellular distribution of LysoTracker red and a lysosomal enzyme, cathepsin D (18), utilizing a fluorescent probe (pepstatin A–BODIPY FL) that binds to cathepsin D (20). Control cells stained with LysoTracker red and pepstatin A–BODIPY FL showed a granular/vesicular pattern consistent with lysosomes (Fig. 4A). The overlay of LysoTracker red and pepstatin A–BODIPY FL–stained cells showed colocalization. After a 0.5-hour incubation with 25 μmol/L of Cu[Dp44mT], the granular, lysosomal type pattern disappeared, with the

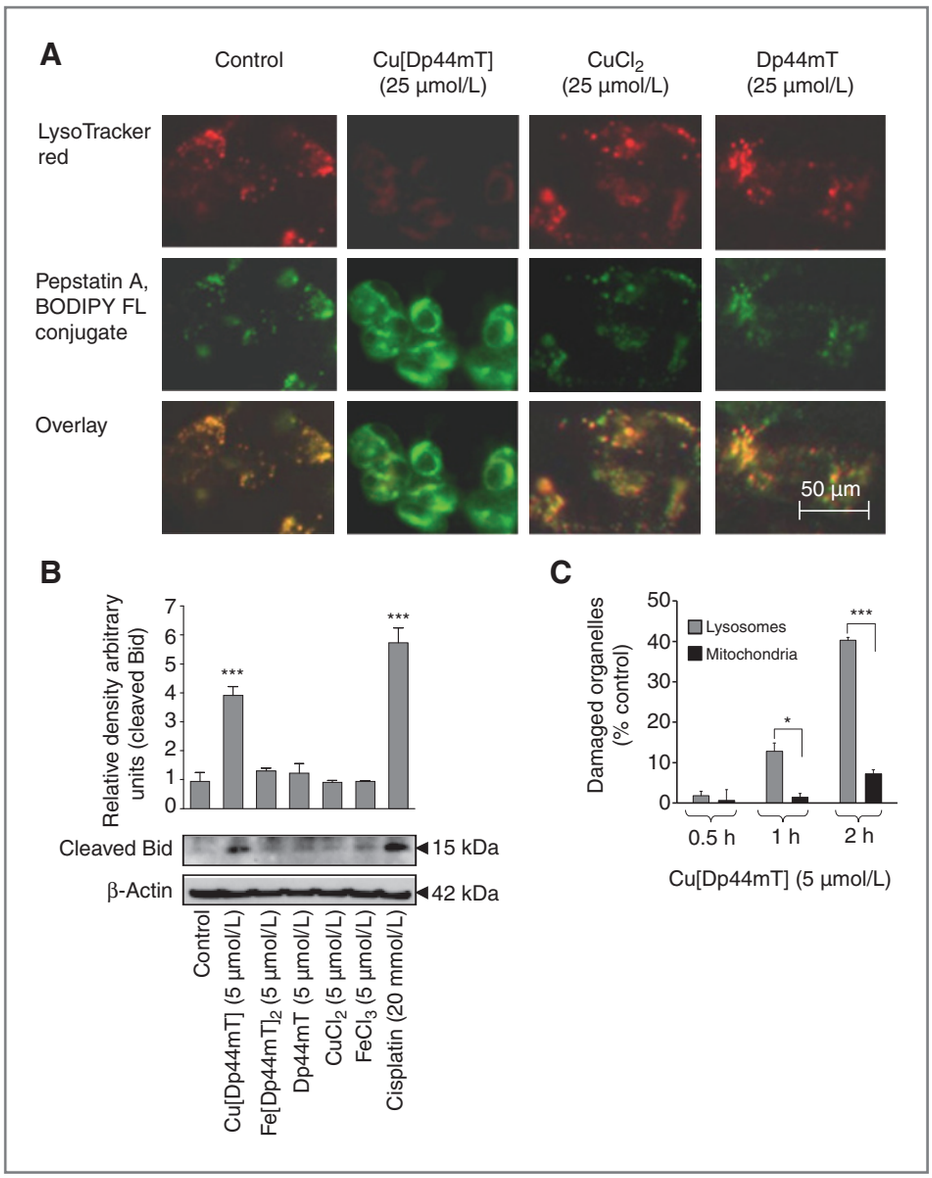

Figure 4. A, a solution of 25 μmol/L of Cu[Dp44mT] causes redistribution of cathepsin D from lysosomes to the cytosol after an incubation of 0.5 hours at 37°C with SK-N-MC cells. Scale bar, 50 μm. Representative images are from 3 experiments. B, Cu[Dp44mT], but not Dp44mT, $Fe[Dp44mT]_2$, $CuCl_2$, or $FeCl_3$, increases cleaved Bid in SK-N-MC cells. The blot is a typical experiment from 3 experiments, whereas the densitometry is mean ± SD (3 experiments). ***, versus control, $P < 0.001$. C, graph showing lysosomal stability compared with mitochondrial stability after 0.5, 1, and 2 hours at 37°C in cells treated with 5 μmol/L of Cu[Dp44mT]. Lysosomal and mitochondrial stability was shown by staining with acridine orange (20 μmol/L) or TMRE (20 nmol/L), respectively, via flow cytometry. Results are mean ± SD (3 experiments). *, lysosomes versus mitochondria, $P < 0.05$; ***, lysosomes versus mitochondria, $P < 0.001$.

fluorescence becoming evenly distributed within the cytosol (Fig. 4A). This observation was consistent with Cu[Dp44mT]-induced LMP, confirming results with acridine orange (Fig. 3D). Neither Cu(II) as $CuCl_2$ (25 μmol/L) or Dp44mT (25 μmol/L) alone had any significant effect on LysoTracker red or cathepsin D staining (Fig. 4A).

To show a relationship between altered LMP and apoptosis induction, Western blotting assessed cleavage of the proapoptotic Bcl-2 family member, BH3-interacting domain death agonist (Bid), by lysosomal proteases (ref. 27; Fig. 4B). As a positive control, cells were incubated with cisplatin (20 mmol/L) that induces Bid cleavage (27). SK-N-MC cells incubated with 5 μmol/L of Cu[Dp44mT] or 20 mmol/L of cisplatin for 2 hours showed significant ($P < 0.001$) cleavage of Bid (Fig. 4B). This confirmed redistribution of lysosomal proteases to the cytosol (Fig. 4A) leading to Bid cleavage and provides a direct link between lysosomal damage and apoptosis induction by Cu[Dp44mT].

Cu[Dp44mT] induces damage to lysosomes earlier than mitochondria

We next examined whether mitochondria were also damaged. Mitochondrial stability was determined by measuring the reduction in mitochondrial membrane potential using TMRE (21), whereas LMP was assayed using acridine orange via flow cytometry. As in Fig. 4C, the damage induced by 5 μmol/L of Cu[Dp44mT] to lysosomes was significantly ($P < 0.05$–0.001) more apparent than that to mitochondria after 1 or 2 hours, indicating that lysosomes were more sensitive to Cu[Dp44mT].

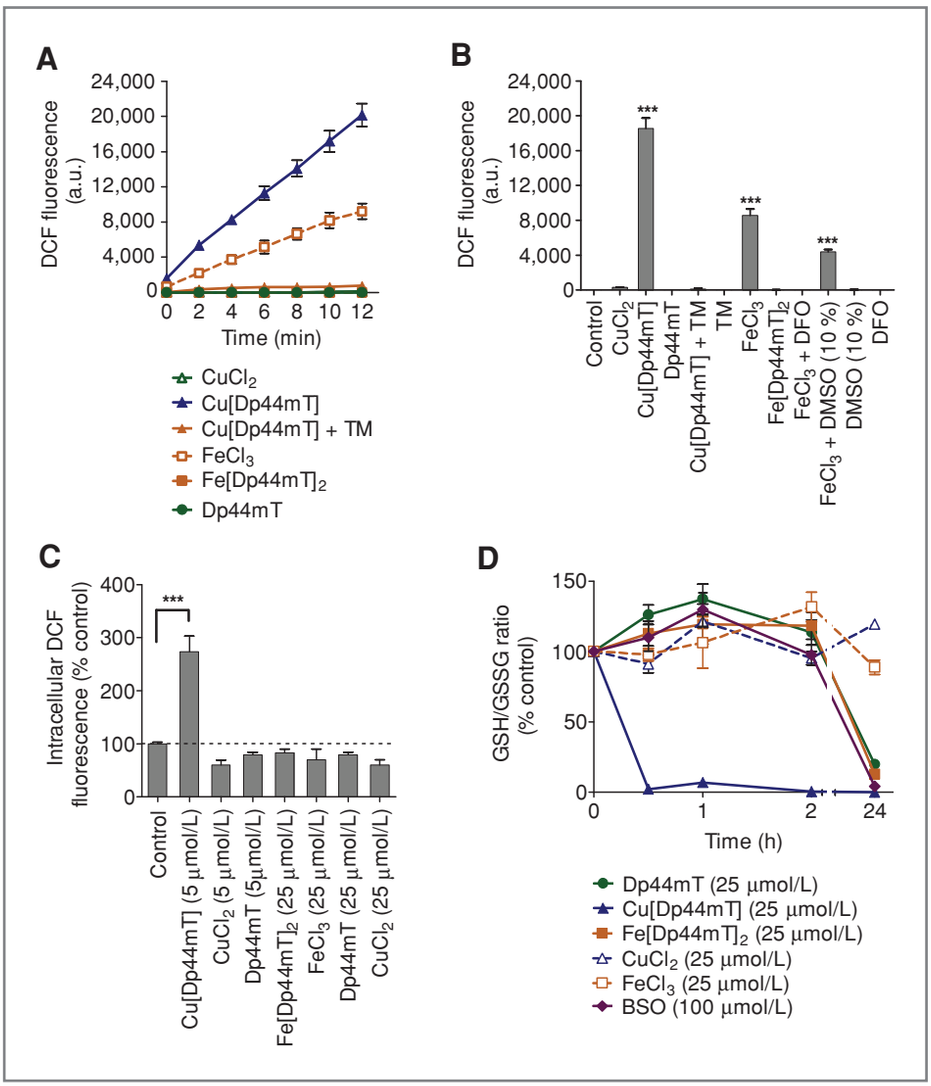

Figure 5. A, hydroxyl radical production by Cu[Dp44mT] relative to $FeCl_3$ and other reagents (at 5 μmol/L, except DMSO which was 10% v/v) as shown by oxidation of nonfluorescent H_2DCF to fluorescent DCF *in vitro* (in solution) under lysosomal like conditions (pH = 5; 100 μmol/L cysteine). B, effect of Cu[Dp44mT] at 5 μmol/L on H_2DCF oxidation after 12 minutes in the presence and absence of various reagents (using the conditions in A). C, intracellular hydroxyl radical generation by 5 μmol/L of Cu[Dp44mT] following an incubation of 0.5 hours at 37°C as shown by flow cytometry using DCF in SK-N-MC cells. D, incubation of SK-N-MC cells for 0.5, 1, 2, or 24 hours at 37°C with Dp44mT, Cu[Dp44mT], $Fe[Dp44mT]_2$, $FeCl_3$, $CuCl_2$ (all 25 μmol/L) or the GSH synthesis inhibitor, BSO (100 μmol/L), reduces the GSH/GSSG ratio. Results are mean ± SD (6 experiments). ***, versus control, $P < 0.001$. a.u., arbitrary units.

Ability of the Cu-Dp44mT and Fe–Dp44mT complexes to generate ROS

To understand why lysosomes were so sensitive to Cu[Dp44mT], we assessed whether the Fe or Cu complexes of Dp44mT generate oxidative stress that could damage lysosomes. These studies in a cell-free system were conducted under lysosomal like conditions at a pH of 5.0 and in the presence of cysteine (ref. 28; Fig. 5A and B). Oxidative stress was determined by the oxidation of nonfluorescent H_2DCF to fluorescent DCF, a well-characterized probe for assessing redox stress (6, 23). The high redox activity of 5 μmol/L of Cu[Dp44mT] was significantly ($P < 0.01$) greater than 5 μmol/L of $CuCl_2$, $FeCl_3$, and $Fe[Dp44mT]_2$ after only 2 minutes (Fig. 5A). Addition of the 5 μmol/L of Cu chelator TM to 5 μmol/L of Cu[Dp44mT] totally prevented its activity, consistent with the ability of TM to bind Cu from Cu[Dp44mT], as shown in Fig. 5A and B.

Considering these results, the potential of Cu[Dp44mT] to induce intracellular ROS in SK-N-MC cells was also assessed using H_2DCF. At 5 μmol/L, Cu[Dp44mT] caused a significant ($P < 0.001$) increase in intracellular H_2DCF oxidation to 273% ± 20% of that found for control cells after a 0.5-hour incubation (Fig. 5C). No increase in H_2DCF oxidation was observed with Cu(II) as $CuCl_2$, Fe(III) as $FeCl_3$, Dp44mT alone, or $Fe[Dp44mT]_2$, even at a 5-fold higher concentration (25 μmol/L; Fig. 5C). Collectively, these experiments show the marked redox activity of Cu[Dp44mT].

Effect of Cu[Dp44mT] on GSH and GSSG levels

To examine the redox activity of Cu[Dp44mT] on physiologic substrates, levels of the well-described indicator of oxidative stress, glutathione (GSH), and oxidized GSH (GSSG; ref. 22) were determined. Over 0.5 to 24 hours incubations with SK-N-MC cells, 25 μmol/L of Cu[Dp44mT] significantly

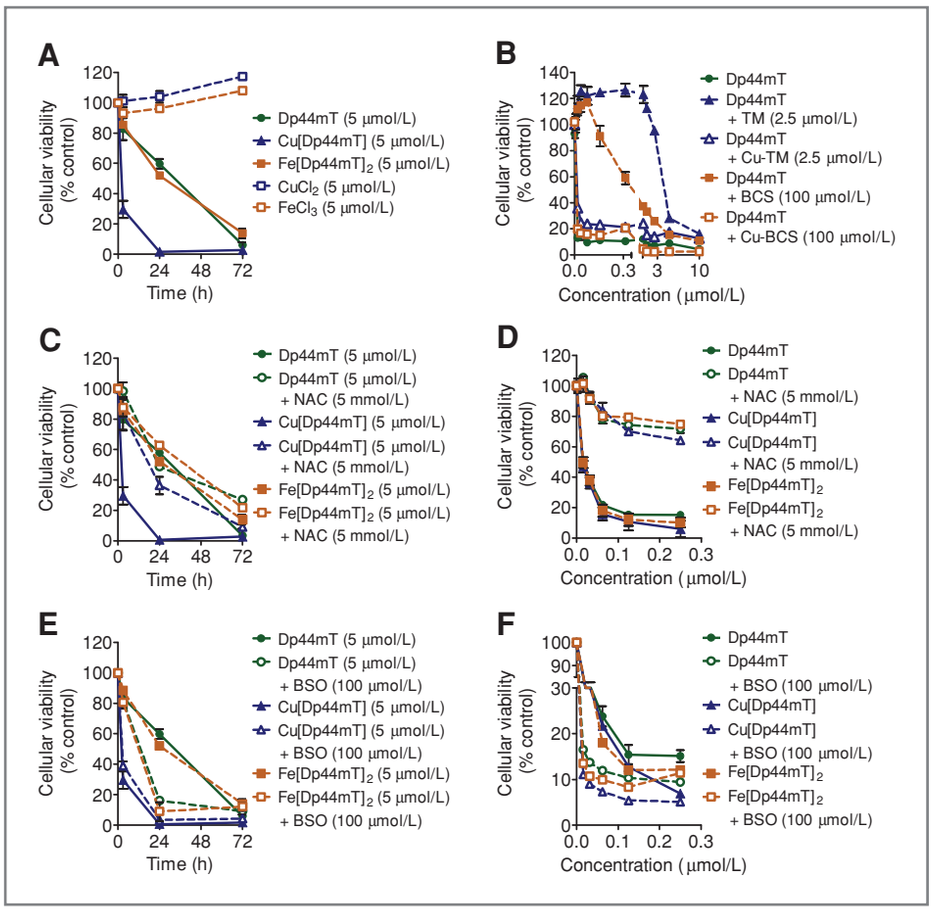

Figure 6. A, cytotoxicity of Cu[Dp44mT] is far more rapid than that of Dp44mT or $Fe[Dp44mT]_2$ at 5 μmol/L using SK-N-MC cells. B, the nontoxic Cu chelators, TM and BCS, reduce Dp44mT cytotoxicity after 72 hours, suggesting that it is mediated by Cu complexation. Results are mean ± SD (5 experiments). C, the GSH precursor, NAC (5 mmol/L), attenuates cytotoxicity of 5 μmol/L of Cu[Dp44mT] and, at 72 hours, reduces Dp44mT (5 μmol/L) cytotoxicity. D, NAC (5 mmol/L) reduces cytotoxicity of Dp44mT, Cu[Dp44mT], and $Fe[Dp44mT]_2$ after 72 hours. E and F, BSO (100 μmol/L), potentiates cytotoxicity of Dp44mT, Cu[Dp44mT], and $Fe[Dp44mT]_2$. The data in F are after a 72-hour incubation. Results are mean ± SD (3 experiments).

($P < 0.001$) reduced the GSH/GSSG ratio to 0% to 7% of the control (Fig. 5D), confirming that Cu[Dp44mT] possesses pronounced redox activity. In comparison, Dp44mT (25 μmol/L), the GSH synthesis inhibitor, BSO (100 μmol/L), or $Fe[Dp44mT]_2$ (25 μmol/L) also reduced the GSH/GSSG ratio to 4% to 20% of the control but only after 24 hours (Fig. 5D).

Cell survival after exposure to Dp44mT and its Cu and Fe complexes

The studies above indicate that Dp44mT enters cells and forms a redox-active Cu complex that damages lysosomes. Considering this, we examined the cytotoxicity of Dp44mT and its Cu and Fe complexes. As shown in Fig. 6A, after a 3-hour incubation, 5 μmol/L of Cu[Dp44mT] significantly ($P < 0.001$) decreased viability to 28% ± 4% of the control. In contrast, Dp44mT or $Fe[Dp44mT]_2$ (both at 5 μmol/L) did not significantly decrease viability within 3 hours but showed activity at 24 hours (Fig. 6A). These results show the pronounced cytotoxicity of Cu[Dp44mT] relative to $Fe[Dp44mT]_2$ or Dp44mT.

Copper chelators, TM and BCS, prevent Dp44mT cytotoxicity

To determine the importance of Cu chelation to the cytotoxicity, we incubated cells for 72 hours at 37°C with increasing Dp44mT concentrations, Dp44mT in the presence of the Cu chelator, TM, or the preformed TM–Cu complex, which blocks the ability of TM to bind cellular Cu (Fig. 6B). The addition of TM to Dp44mT markedly prevented the ability of the latter to reduce cellular viability up to a Dp44mT concentration of 2.5 μmol/L, whereas the preformed Cu-TM complex (which cannot bind cellular Cu) had no significant rescue effect on Dp44mT cytotoxicity (Fig. 6B).

To confirm that the ability of TM to rescue Dp44mT cytotoxicity was due to Cu chelation, we used the structurally unrelated Cu chelator, bathocuproine disulfonate (BCS), in identical studies and observed a similar, but less pronounced, rescue effect on Dp44mT cytotoxicity (Fig. 6B). Like TM, BCS decreased Dp44mT cytotoxicity, whereas its Cu complex (BCS-Cu) had no significant influence (Fig. 6B), as its binding site was saturated with Cu. Notably, BCS or TM alone or their Cu complexes had no significant effect on viability (Supplementary Fig. S3).

As Dp44mT concentration increased, the ability of the Cu chelators BCS or TM to prevent cytotoxicity was markedly reduced after 72 hours (Fig. 6B). This may reflect chelation of Fe by Dp44mT which becomes significant at these higher concentrations and leads to Fe deprivation and cytotoxicity (6). Indeed, while the binding of Cu by Dp44mT is crucial for its antitumor efficacy, its Fe chelation efficacy is also important (6, 8).

GSH levels modulate Cu[Dp44mT] cytotoxicity

Because GSH plays an important role in buffering redox stress (22) and considering the marked redox activity of Cu[Dp44mT], as shown in Fig. 5A–C, further studies examined its effect on GSH (Fig. 6C–F). To investigate this, the effect of GSH supplementation or depletion on viability was assessed by incubating cells in the presence of *N*-acetylcysteine (NAC) that enhances GSH levels (22), or the GSH synthesis inhibitor, BSO, that decreases GSH (22). Indeed, a 24-hour incubation of SK-N-MC cells with NAC (5 mmol/L) or BSO (100 μmol/L) significantly ($P < 0.001$) increased and decreased the GSH/GSSG ratio to 155% ± 5% and 4% ± 2% ($n = 3$) of the control, respectively.

The addition of NAC (5 mmol/L) with Cu[Dp44mT] significantly ($P < 0.001$) prevented the decrease in viability due to Cu[Dp44mT] after 3 and 24 hours (Fig. 6C), and similar results were observed as a function of concentration over 72 hours (Fig. 6D). Supplementation with NAC also significantly ($P < 0.01$) protected against the decreased viability observed with $Fe[Dp44mT]_2$ or Dp44mT alone after 72 hours (Fig. 6C and D), and thus decreased their cytotoxicity. Further, morphologic studies using acridine orange also showed that NAC preserved lysosomal integrity in the presence of Cu[Dp44mT], as shown in Supplementary Fig. S4.

In contrast to NAC, the addition of BSO with Dp44mT and $Fe[Dp44mT]_2$ significantly ($P < 0.001$) enhanced their cytotoxicity particularly at 24 hours (Fig. 6E). However, the addition of BSO with 5 μmol/L of Cu[Dp44mT] did not increase its cytotoxicity (Fig. 6E). This may be due to the marked redox activity of Cu[Dp44mT] relative to Dp44mT and $Fe[Dp44mT]_2$ at high concentrations (Fig. 5A), which rapidly depresses GSH levels (Fig. 5D).

As a function of chelator or complex concentration (0.02–0.25 μmol/L), BSO potentiated cytotoxicity of Dp44mT, $Fe[Dp44mT]_2$, and Cu[Dp44mT] after 72 hours (Fig. 6F). Hence, at low Cu[Dp44mT] concentrations (i.e., 0.02–0.25 μmol/L; Fig. 6F), BSO clearly potentiated the cytotoxicity of this complex after 72 hours, in contrast to higher Cu[Dp44mT] concentrations (i.e., 5 μmol/L; Fig. 6E).

Discussion

In this investigation, we showed that incubation of cells with Dp44mT leads to retention of its ^{64}Cu complex. The probable reason for this is the ionization characteristics of Dp44mT (8). At physiologic pH, Dp44mT is neutral and permeates cell membranes (6, 8). However, in the lysosomal compartment (pH ~5; ref. 29), an increased proportion of Dp44mT becomes positively charged leading to accumulation, ROS formation, and LMP.

Dp44mT induces apoptosis using several cell types and a tumor model *in vivo* (6). Moreover, we showed that apoptosis occurred via the mitochondrial pathway, where decreased Bcl-2 and increased Bax expression occurred along with holocytochrome *c* (h-cyt*c*) release and caspase activation (6). Our study suggests that these apoptotic events could be caused by Cu[Dp44mT]-induced redox stress that results in LMP, causing redistribution of lysosomal cathepsins to the cytosol (Fig. 4A) and concomitant cleavage of Bid into its proapoptotic form (Fig. 4B). Indeed, cathepsins can cleave Bid, which migrates to mitochondria and induces outer membrane permeabilization that is dependent on proapoptotic Bax (30). Bax plays a role in inducing release of mitochondrial h-cyt*c*, thereby activating the caspase cascade (31), which we showed occurs after Dp44mT treatment (6). Hence, LMP by redox-active Cu[Dp44mT] could result in downstream effects on mitochondria that lead to h-cyt*c* release.

The Dp44mT-Cu complex showed far greater cytotoxicity as a function of time than either the Fe complex or the ligand alone. This was also reflected in the faster kinetics of lysosomal rupture (Fig. 3D), cathepsin D release (Fig. 4A), and decrease in GSH/GSSG ratio (Fig. 5D) induced by Cu[Dp44mT]. As these events all occur over the same time scale, they suggest a coherent and coordinated series of events that ultimately induces significant cytotoxicity. Intriguingly, the importance of Cu in mediating the cytotoxicity of the free ligand was shown by the rescue effect of the nontoxic Cu chelators, TM and BCS. This indicated that formation of a redox-active Cu[Dp44mT] complex is important for Dp44mT activity. Moreover, it was shown that Cu[Dp44mT] results in a marked decrease in GSH and the cytotoxicity of this complex can be reduced by NAC, which enhances GSH levels (22). Conversely, cytotoxicity can be potentiated by the GSH inhibitor, BSO. These results indicate that lysosomal damage caused by Cu[Dp44mT] was directly due to its redox activity. On the basis of these data, we propose a model of the mechanism of action of Dp44mT (Fig. 7).

Another aspect of the mechanism of action of Dp44mT is that it shows selectivity against tumor cells *in vitro* and *in vivo* (7). The basis for this relates, in part, to the greater uptake and metabolism of Cu and Fe for essential processes in cancer cells relative to normal cells (5). Under such conditions, the lysosome could be more active in terms of its metal metabolism, and hence, more susceptible to Dp44mT. It is also known that lysosomal autophagic pathways in cancer cells are abnormal due to the monoallelic deletion of the essential autophagy

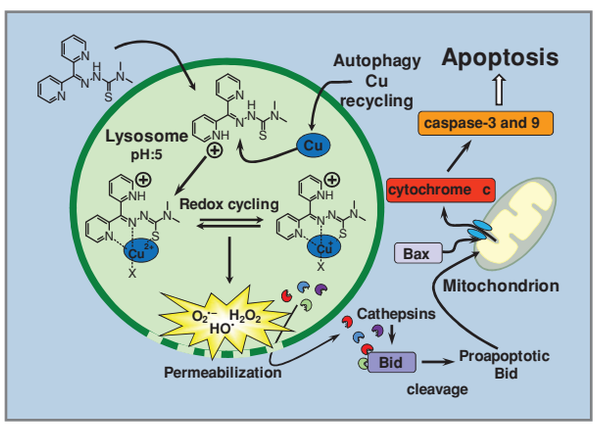

Figure 7. Lysosomal targeting by Dp44mT. Because of its ionization properties, Dp44mT becomes trapped in acidic lysosomes and binds Cu to form a redox-active complex that causes LMP and subsequently apoptosis.

regulator, *beclin1* (32). As such, metal recycling due to autophagy could be disturbed and lead to differences between neoplastic and normal cells in their response to agents such as Dp44mT.

In summary, we have dissected the mechanism of action of Dp44mT and showed that it accumulates in lysosomes due to its unique ionization characteristics. Our investigation reveals the marked redox activity of Cu[Dp44mT] leads to LMP that induces cell death. Moreover, this study shows that targeting lysosomes can lead to potent and selective anticancer therapeutics. Knowledge of this mechanism can be used to design more potent cytotoxic agents that affect the lysosomal apoptosis pathway.

Disclosure of Potential Conflicts of Interest

No potential conflicts of interest were disclosed.

Acknowledgments

D.R. Richardson thanks the National Health and Medical Research Council for a Senior Principal Research Fellowship and Project Grant support. D.B. Lovejoy and P.J. Jansson thank the Cancer Institute NSW for Fellowship support.

The costs of publication of this article were defrayed in part by the payment of page charges. This article must therefore be hereby marked *advertisement* in accordance with 18 U.S.C. Section 1734 solely to indicate this fact.

Received April 11, 2011; revised June 15, 2011; accepted June 29, 2011; published OnlineFirst July 12, 2011.

References

1. Yu Y, Wong J, Lovejoy DB, Kalinowski DS, Richardson DR. Chelators at the cancer coalface: desferrioxamine to Triapine and beyond. Clin Cancer Res 2006;12:6876–83.
2. Morgan EH. Transferrin biochemistry, physiology and clinical significance. Mol Aspects Med 1981;4:1–23.
3. Trinder D, Zak O, Aisen P. Transferrin receptor-independent uptake of differic transferrin by human hepatoma cells with antisense inhibition of receptor expression. Hepatology 1996;23:1512–20.
4. Gupte A, Mumper RJ. Elevated copper and oxidative stress in cancer cells as a target for cancer treatment. Cancer Treat Rev 2009;35:32–46.
5. Pahl PM, Horwitz LD. Cell permeable iron chelators as potential cancer chemotherapeutic agents. Cancer Invest 2005;23:683–91.
6. Yuan J, Lovejoy DB, Richardson DR. Novel di-2-pyridyl-derived iron chelators with marked and selective antitumor activity: *in vitro* and *in vivo* assessment. Blood 2004;104:1450–8.
7. Whitnall M, Howard J, Ponka P, Richardson DR. A class of iron chelators with a wide spectrum of potent antitumor activity that overcomes resistance to chemotherapeutics. Proc Natl Acad Sci U S A 2006;103:14901–6.
8. Richardson DR, Sharpe PC, Lovejoy DB, Senaratne D, Kalinowski DS, Islam M, et al. Dipyridyl thiosemicarbazone chelators with potent and selective antitumor activity form iron complexes with redox activity. J Med Chem 2006;49:6510–21.
9. Jansson PJ, Hawkins CL, Lovejoy DB, Richardson DR. The iron complex of Dp44mT is redox-active and induces hydroxyl radical formation: an EPR study. J Inorg Biochem 2010;104:1224–8.
10. Rao VA, Klein SR, Agama KK, Toyoda E, Adachi N, Pommier Y, et al. The iron chelator Dp44mT causes DNA damage and selective inhibition of topoisomerase IIalpha in breast cancer cells. Cancer Res 2009;69:948–57.
11. Tian J, Peehl DM, Zheng W, Knox SJ. Anti-tumor and radiosensitization activities of the iron chelator HDp44mT are mediated by effects on intracellular redox status. Cancer Lett 2010;298:231–7.
12. Rao VA, Zhang J, Klein SR, Espandiari P, Knapton A, Dickey JS, et al. The iron chelator Dp44mT inhibits the proliferation of cancer cells but fails to protect from doxorubicin-induced cardiotoxicity in spontaneously hypertensive rats. Cancer Chemother Pharmacol 2011 Mar 4. [Epub ahead of print].
13. Jansson PJ, Sharpe PC, Bernhardt PV, Richardson DR. Novel thiosemicarbazones of the ApT and DpT series and their copper complexes: identification of pronounced redox activity and characterization of their antitumor activity. J Med Chem 2010;53:5759–69.
14. van den Berghe PV, Folmer DE, Malingré HE, van Beurden E, Klomp AE, van de Sluis B, et al. Human copper transporter 2 is localized in late endosomes and lysosomes and facilitates cellular copper uptake. Biochem J 2007;407:49–59.
15. Kurz T, Terman A, Gustafsson B, Brunk UT. Lysosomes in iron metabolism, ageing and apoptosis. Histochem Cell Biol 2008;129:389–406.
16. Pourahmad J, Ross S, O'Brien PJ. Lysosomal involvement in hepatocyte cytotoxicity induced by Cu(2+) but not Cd(2+). Free Radic Biol Med 2001;30:89–97.
17. Richardson DR, Tran EH, Ponka P. The potential of iron chelators of the pyridoxal isonicotinoyl hydrazone class as effective antiproliferative agents. Blood 1995;86:4295–306.
18. Yu H, Zhou Y, Lind SE, Ding WQ. Clioquinol targets zinc to lysosomes in human cancer cells. Biochem J 2009;417:133–9.
19. Persson HL, Kurz T, Eaton JW, Brunk UT. Radiation-induced cell death: importance of lysosomal destabilization. Biochem J 2005;389:877–84.
20. Chen CS, Chen WN, Zhou M, Arttamangkul S, Haugland RP. Probing the cathepsin D using a BODIPY FL-pepstatin A: applications in fluorescence polarization and microscopy. J Biochem Biophys Methods 2000;42:137–51.
21. Scaduto RC Jr, Grotyohann LW. Measurement of mitochondrial membrane potential using fluorescent rhodamine derivatives. Biophys J 1999;76:469–77.
22. Meister A, Anderson ME. Glutathione. Annu Rev Biochem 1983;52:711–60.
23. Myhre O, Andersen JM, Aarnes H, Fonnum F. Evaluation of the probes 2′,7′-dichlorofluorescin diacetate, luminol, and lucigenin as indicators of reactive species formation. Biochem Pharmacol 2003;65:1575–82.
24. Aschwood-Smith MJ. Current concepts concerning radioprotective and cryoprotective properties on dimethyl sulfoxide in cellular systems. Ann NY Acad Sci 1967;141:41–62.
25. Del Maestro R, Thaw HH, Bjork J, Planker M, Arfors KE. Free radicals as mediators of tissue injury. Acta Physiol Scand Suppl 1980;492:91–119.
26. Brewer GJ, Dick RD, Grover DK, LeClaire V, Tseng M, Wicha M, et al. Treatment of metastatic cancer with tetrathiomolybdate, an anticopper, antiangiogenic agent: phase I study. Clin Cancer Res 2000;6:1–10.
27. Mandic A, Viktorsson K, Strandberg L, Heiden T, Hansson J, Linder S, et al. Calpain-mediated Bid cleavage and calpain-independent Bak modulation: two separate pathways in cisplatin-induced apoptosis. Mol Cell Biol 2002;22:3003–13.
28. Pisoni RL, Acker TL, Lisowski KM, Lemons RM, Thoene JG. A cysteine-specific lysosomal transport system provides a major route for the delivery of thiol to human fibroblast lysosomes: possible role in supporting lysosomal proteolysis. J Cell Biol 1990;110:327–35.
29. de Duve C. Lysosomes revisited. Eur J Biochem 1983;137:391–7.
30. Billen LP, Shamas-Din A, Andrews DW. Bid: a Bax-like BH3 protein. Oncogene 2008;27Suppl 1:S93–104.
31. Chalah A, Khosravi-Far R. The mitochondrial death pathway. Adv Exp Med Biol 2008;615:25–45.
32. Chen N, Karantza-Wadsworth V. Role and regulation of autophagy in cancer. Biochim Biophys Acta 2009;1793:1516–23.